$ZrGeTe_4$ Nanoparticles as Saturable Absorber for Mode-Locking Operations at 1 and 1.55 μm

Xinxin Shang , Nannan Xu , Mengyu Zong , Weiyi Yu , Linguang Guo , Guanguang Gao , Ziqi Zhang , Huanian Zhang * , Lianzheng Su *

Posted Date: 16 March 2026

doi: 10.20944/preprints202603.1241.v1

Keywords: ultrafast fiber laser; saturable absorber; passive mode-locked; $ZrGeTe_4$ nanoparticles

Article

$ZrGeTe_4$ Nanoparticles as Saturable Absorber for Mode-Locked Operations at 1 and 1.55 μm

Xinxin Shang [1,2], Nannan Xu [1,2], Mengyu Zong [1,2], Weiyi Yu [1], Linguang Guo [3], Guanguang Gao [4], Ziqi Zhang [5], Huanian Zhang [5,6,*] and Lianzheng Su [1,*]

[1] School of Medical Imaging, Qilu Medical University, Zibo 255300, China
[2] School of Physics and Electronics, Shandong Normal University, Jinan 250014, China
[3] State Key Laboratory on Tunable Laser Technology, Department of Electronics and Information Engineering, Harbin Institute of Technology (Shenzhen), Shenzhen 518055, China
[4] Shanghai Institute of Optics and Fine Mechanics, Chinese Academy of Sciences, Shanghai 201800, China
[5] School of Physics and Optoelectronic Engineering, Shandong University of Technology, Zibo 255049, China
[6] Zhejiang Deeper Celler Medical Equipment Co., Ltd, Wenling 317500, China
* Correspondence: huanian_zhang@163.com (H.Z.); xiulianzheng@qlmu.edu.cn (L.S.)

Abstract

In the current paper, the nonlinear absorption characteristics and laser modulation performance of the ternary anisotropic semiconductor material $ZrGeTe_4$ were successfully explored. The recovery time of the $ZrGeTe_4$-PVA thin film was measured to be 5.74 ps by pump-probe technology. By employing $ZrGeTe_4$ as a saturable absorber, a passive mode-locked Yb-doped fiber laser was demonstrated for the first time. In the 1 μm mode-locked operation, the central wavelength is 1031.29 nm, the pulse repetition rate is 24.85 MHz, and the pulse width is 786.3 ps. In an Er-doped fiber laser operating at the wavelength of 1561.10 nm, the pulse width as short as 1.26 ps with a repetition rate of 4.38 MHz. The results show that $ZrGeTe_4$ has excellent broadband nonlinear optical characteristics.

Keywords: ultrafast fiber laser; saturable absorber; passive mode-locked; $ZrGeTe_4$ nanoparticles

1. Introduction

Near-infrared (NIR) pulsed fiber laser sources have been widely applied in precision micro-processing, optical communication, biomedicine, nonlinear dynamics, etc [1–5]. The pulsed laser in the 1 μm band can achieve high pulse energy and peak power output due to its high conversion efficiency, making it widely used in the research of ultra-fast dynamics of materials by serving as a pump source [6]. Moreover, the 1 μm band laser is widely used in multi-photon imaging and biomedical treatment. For instance, Wang et al. successfully distinguished the distribution of water and fat in tissues using a dual-wavelength of 1064 nm and 1176 nm, opening up new directions for metabolic monitoring [7]. The 1.55 μm band laser is in the communication band, compared with other lasers, it can provide a broader bandwidth, higher gain, and reduced attenuation. They have excellent performance in long-distance fiber transmission and thus have significant research value [8]. Additionally, the 1.55 μm band pulsed fiber laser is the most typical dissipative system, containing periodic gain, loss, dispersion, and nonlinear effects. It is the most commonly used tool for exploring temporal and spatial mode-locking, various new optical soliton phenomena, and their interactions [9,10]. It is also widely regarded as a pump source for the 1.7 μm band laser applied in the medical industry [11]. Therefore, the 1 μm and 1.55 μm fiber lasers are two important and most researched bands in the near-infrared spectrum.

Pulsing in fiber lasers may be achieved by many approaches, such as Gain-Switching, Actively Q-switching and Mode-locking (Electro-optic modulator and Acousto-optic modulation), and Optical Switches, although passively mode-locking probably the most prevalent [12–15]. So far, various nanomaterials have been employed widely as saturable absorbers (SAs) in passively mode-

 doi:10.20944/preprints202603.1241.v1

locking fiber lasers to generate ultra-short pulses, such as carbon nanotube (CNT), graphene, black phosphorus (BP), topological insulator (TI) and transition metal dichalcogenides (TMDs) [16–22]. Two-dimensional (2D) materials possess unique atomic-layer structures and exhibit superior nonlinear optical absorption properties compared to traditional bulk materials. In particular, their ultrafast carrier dynamics and tunable bandgap structure provide a new platform for generating ultra-short pulse laser pulses [23,24]. To obtain better-performance broadband passive mode-locked fiber lasers, researchers should explore new nonlinear nanomaterials as SAs.

$ZrGeTe_4$ is a kind of layered ternary semiconductor compound with tunable bandgap, whose bandgap varies with the number of layers [25,26]. Few-layer $ZrGeTe_4$ and bulk $ZrGeTe_4$ are indirect bandgap semiconductors, while single-layer $ZrGeTe_4$ has been proven to be a direct bandgap semiconductor [27]. The band gap value of the few-layer $ZrGeTe_4$ varies with the number of layers and decreases as the number of layers increases. Its single-layer structure exhibits a direct bandgap of 0.686 eV. The structure from the 2_{nd} layer to the 5_{th} layer exhibits a direct band gap, with the band gap value ranging from 0.339 eV to 0.536 eV [28]. The spacing between adjacent layers is 0.82 nm [29]. The van der Waals forces between layers are relatively weak, which means that $ZrGeTe_4$ materials with only a few layers or a single layer can be fabricated through simple exfoliation methods (such as liquid-phase exfoliation). The nonlinear optical properties of $ZrGeTe_4$ have been reported in the 1.55 μm wavelength range, but there is a lack of research in the 1 μm wavelength range [28,30,31]. Therefore, it is of great significance to prove that $ZrGeTe_4$ is a nonlinear optical material with broadband saturated absorption characteristics.

This study demonstrated the application of $ZrGeTe_4$ SA material for generating mode-locked pulses in Yb-doped fiber laser at a working wavelength of 1 μm and Er-doped fiber laser at 1.55 μm. The modulation depth of the $ZrGeTe_4$-polyvinyl alcohol (PVA) film SA prepared by the liquid-phase exfoliation method is 7.7% at 1031 nm and 14.5% at 1561 nm, respectively. Based on $ZrGeTe_4$ SA, we have achieved mode-locked operation in a ytterbium-doped fiber laser for the first time, with a central wavelength of 1031.29 nm, a pulse repetition rate of 24.85 MHz, and a pulse width of 786.3 ps. In the highly stable mode-locked Er-doped fiber laser, the central wavelength located at 1561.10 nm, the pulse width is 1.26 ps, and the pulse repetition frequency is 4.38 MHz. The results demonstrate that $ZrGeTe_4$ SA possess distinct advantages for the development of high-efficiency, highperformance and broadband multi-wavelengths fiber lasers.

2. Characterization and Synthesis of the $ZrGeTe_4$ Nanoparticles

Through means such as scanning electron microscopy (SEM), transmission electron microscopy (TEM), X-ray diffraction (XRD), Raman spectrum, energy-dispersion X-ray spectroscopy (EDS), and atomic force microscopy (AFM), it has been confirmed that large-scale, multi-layer $ZrGeTe_4$ nanoparticles with high quality have been formed. The film-formable saturable absorber was prepared by the liquid-phase exfoliation method. Through the I-scan technology, the modulation depth, saturation intensity and non-saturable absorbance at wavelengths of 1 μm and 1.55 μm were measured. The recovery time was measured by using the pump-probe detection technique.

To investigate the surface characteristics of the prepared $ZrGeTe_4$ nanoparticles, it was characterized by using the SEM (Sigma 500, ZEISS, Oberkochen, Germany), revealing a distinct layered structure. Figure 1a presents the SEM microscopic image of the vertical direction of $ZrGeTe_4$ at a resolution of 2 μm. Obvious lamellar structures can be observed. Figure 1b is a detailed view, showing that the morphology of $ZrGeTe_4$ has clear and irregular particle boundaries. Figure 1c presents the SEM microscopic image of the horizontal direction of $ZrGeTe_4$ at a resolution of 2 μm. Figure 1d is an enlarged view of the area shown in Figure 1c. There is a distinct layered phenomenon, indicating that the $ZrGeTe_4$ nanoparticles have anisotropic nature.

 doi:10.20944/preprints202603.1241.v1

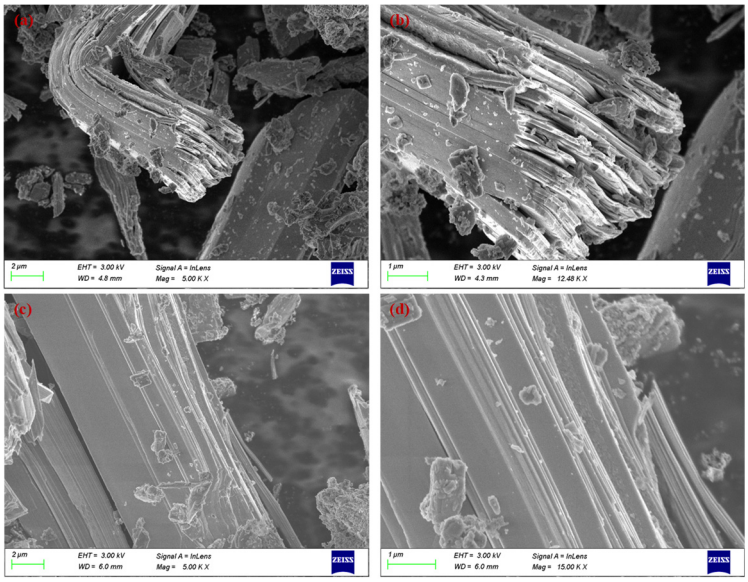

Figure 1. SEM image of $ZrGeTe_4$ nanoparticles.

The morphology and layered structure of $ZrGeTe_4$ nanoparticles were characterized by a TEM (JEM-2100, JEOL, Tokyo, Japan). Figure 2a shows that $ZrGeTe_4$ nanoparticles with the optical resolution of 100 nm confirms their high purity. As shown in Figure 2b, the $ZrGeTe_4$ nanoparticles exhibit distinct lattice stripes, and at their edges, an irregularly shaped sheet-like structure is observed. The $ZrGeTe_4$ nanoparticles sample were analyzed by XRD (D8 Advance, Bruker, Billerica, MA, USA). The results are shown in Figure 2c, where the diffraction peaks are observed at positions (020), (040), (060), and (080), respectively, which is consistent with previous reports [31]. Figure 2d presents the Raman spectrum of $ZrGeTe_4$ nanoparticles. From the Raman spectrum, three characteristic peaks can be observed, located at 91 cm^{-1}, 120 cm^{-1}, and 150 cm^{-1} respectively.

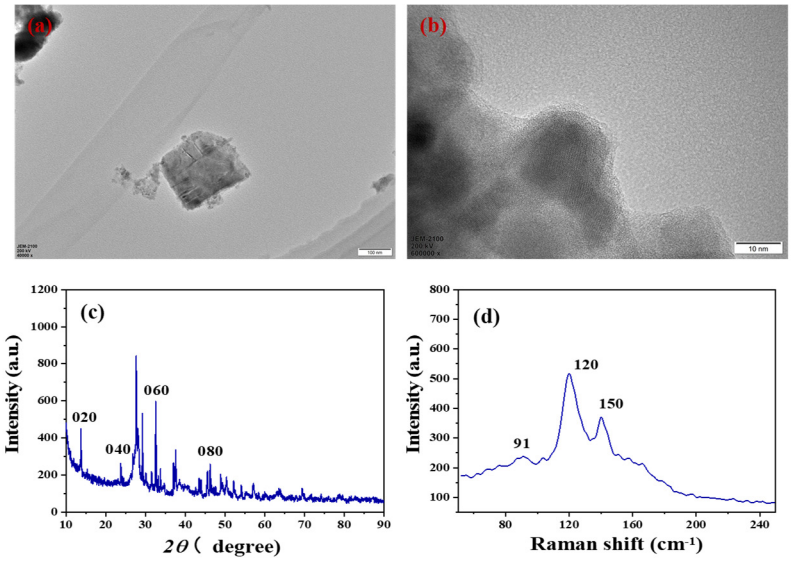

Figure 2. (a) TEM image. (b) HR-TEM image. (c) XRD. (d) Raman spectrum.

Figure 3a-e display the element distribution map and spectral map of $ZrGeTe_4$ nanoparticles. Figure 3a shows the SEM image of selected area layered $ZrGeTe_4$ nanoparticles. The element mapping images obtained through EDS (QUANTAX EDS, Bruker, Germany) surface scanning analysis are shown in Figure 3b-d, where Zr, Ge, and Te are represented by different colors, and the regional distribution is clearly visible, indicating that the $ZrGeTe_4$ nanoparticles we used is very pure. Figure

 doi:10.20944/preprints202603.1241.v1

3e represents the signal peaks of the elements Zr, Ge, and Te, respectively, the atomic ratio is close to 1:1:4, demonstrating the uniform distribution of these three elements. AFM (Multimode 8, Bruker, Germany) is employed to measure the thickness of the $ZrGeTe_4$ nanoparticles, as shown in Figure 3f. The illustration reveals that the thickness of the prepared $ZrGeTe_4$ sample is 3 nm. Since the thickness of a single layer of $ZrGeTe_4$ material is approximately 0.82 nm, the thickness of the prepared $ZrGeTe_4$ sample is approximately 4 layers.

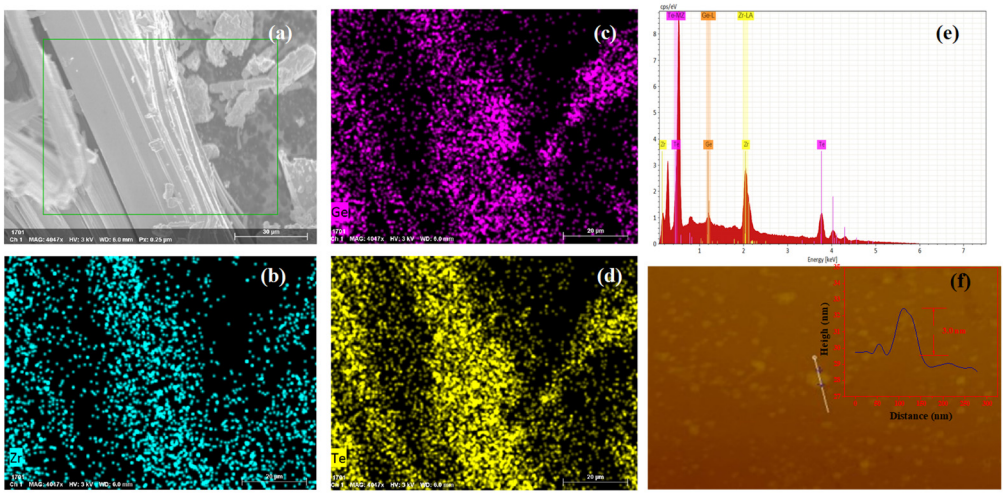

Figure 3. (a) The corresponding SEM image. (b-d) Elemental mapping corresponding to the EDS surface scanning analysis of Zr, Ge, and Te in $ZrGeTe_4$. (e) EDS point scanning analysis image of $ZrGeTe_4$ material. (f) AFM image.

The preparation process of the $ZrGeTe_4$-PVA film SA is shown in Figure 4a. Grind the bulk $ZrGeTe_4$ into fine powder in an agate grinding bowl. Firstly, 50 mg of $ZrGeTe_4$ powder was added to 100 ml of anhydrous ethanol, and a layered $ZrGeTe_4$ nanosheet dispersion was successfully prepared by ultrasonic cleaning for 48 hours. A portion of the sample was taken for characterization and detection. Secondly, a 6% (volume ratio) polyvinyl alcohol solution was mixed with the $ZrGeTe_4$ dispersion at a volume ratio of 1:1 and treated in an ultrasonic cleaner for 24 hours. Then, the uniform $ZrGeTe_4$-PVA solution was spin-coated onto a glass slide, which was placed in a drying oven at 30°C for 12 hours to obtain an $ZrGeTe_4$-PVA film. Finally, a 1 mm × 1 mm $ZrGeTe_4$-PVA film was cut as a SA and transferred to the end of an optical fiber jumper. Using an FC/PC connector to couple the single-mode fiber containing the SA with another clean single-mode fiber jumper.

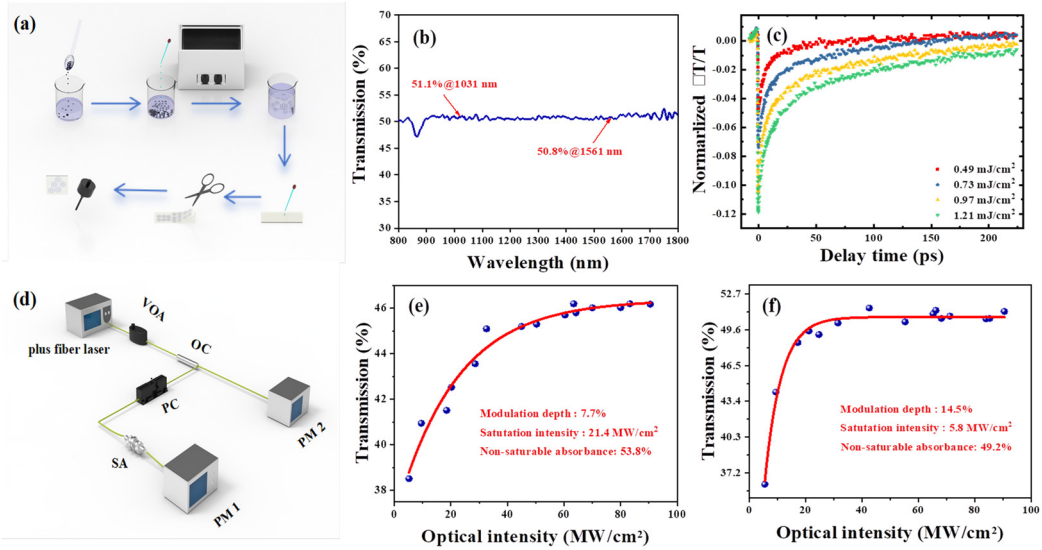

 doi:10.20944/preprints202603.1241.v1

Figure 4. (a)Synthesis procedure of $ZrGeTe_4$ -PVA SA. (b) Linear transmission spectra of $ZrGeTe_4$ -PVA SA at different wavelengths. (c) Transient reflectivity change of $ZrGeTe_4$-PVA thin film under pump fluence densities ranging from 0.49 to 1.21 mJ/cm^2. (d) The experimental setup used for testing nonlinear optical properties. (e) Non-linear absorption measurements of the $ZrGeTe_4$ -PVA SA at 1 μm. (f) Non-linear absorption measurements of the $ZrGeTe_4$ -PVA SA at 1.55 μm.

The linear transmittance spectrum was analyzed using an ultraviolet/visible/near-infrared (UV/vis/NIR) spectrophotometer ((U-4100, Hitachi, Tokyo, Japan) within the range of 800 nm to 1800 nm to characterize the absorption properties of the prepared $ZrGeTe_4$-PVA thin film. As shown in Figure 4b, the transmittance of the film was measured to be 51.1 % at 1031 nm and approximately 50.8 % at 1561 nm. Due to the bandgap of $ZrGeTe_4$, its relatively broad optical absorption band ensures its potential light absorption capability in the near-infrared range. In addition, we conducted high energy fluence pump-probe experiments at the laser amplification stage (Ascend, 800 nm, 35 fs, 5 kHz) (Solstice Ace, Spectra-Physics, CA, USA). The pump energy fluence ranged from 0.49 to 1.21 mJ/cm^2, as can be seen from the figure 4c, the kinetic curves of $ZrGeTe_4$ thin film with different thicknesses are similar. After fitting the relaxation part with a single exponential function, the carrier lifetime or relaxation time is approximately 5.74 ps. The nonlinear optical properties of $ZrGeTe_4$-PVA thin film SA were measured using I-scan technology, and the experimental setup is shown in Figure 4d. The light source for I-scan measurement was a self-made 1 μm and 1.55 μm pulsed fiber laser. In the I-scan experiment, the incident laser intensity was controlled by adjusting the optical attenuator. The beam splitter divided the probe laser into two beams, and two identical power meters were used to simultaneously record the transmittance under different incident power densities. The experimental data were fitted using the following equation:

$$T(I) = 1 - T_{ns} - \Delta T \times \exp\left(-I/I_{sat}\right) \quad (1)$$

in which $T(I)$ and T_{ns} are the nonsaturable loss and transmission rate, respectively, I and I_{sat} are the saturation intensity and input pulse energy, respectively, and ΔT is the modulation depth. As described in Figure 4e and 4f, the fitting results yields modulation depths of 7.7 % and 14.5 %, saturation intensities of 21.4 MW/cm^2 and 5.8 MW/cm^2, and non-saturable absorbance of 53.8 % and 49.2 % for the $ZrGeTe_4$-PVA thin film SA at 1 μm and 1.55 μm, respectively. Furthermore, in mode-locked fiber lasers, a smaller modulation depth can effectively suppresses Q-switched mode-locking and reduces the start-up threshold, enabling highly efficient and stable continuous-wave mode-locked laser operation. These results highlight the nonlinear optical potential of $ZrGeTe_4$ and contribute valuable insight into the development of cost-effective and sensitive mode-locking devices.

3. Experimental Setup

The scheme of the fiber-ring cavity that incorporates the $ZrGeTe_4$-SA is shown in Figure 5. A laser diode (LD)(Taizhou Tonghe Laser technology co. LTD, Wenling, China) operating at 980 nm in the CW regime was used as a pumping source. The wavelength division multiplexer (WDM) was spliced with a pump and the other port was spliced with the gain fiber. The length of the ytterbium-doped optical fiber (LIEKKI Yb1200, nlight, Vancouver, WA, USA) is 30 cm, and the length of the erbium-doped optical fiber (LIEKKI Er110, nlight, Vancouver, WA, USA) is 40 cm. The total cavity lengths of the ytterbium-doped fiber laser and the erbium-doped fiber laser are 8.27 meters and 46.63 meters, respectively. A polarization controller (PC) was employed to change the polarization state of the laser. The generated fiber laser was extracted through an optical coupler (OC) with 10% output for monitoring. Unidirectional light propagation was maintained inside the cavity using a polarization-independent isolator (PI-ISO). Then, $ZrGeTe_4$-PVA thin film SA was incorporated inside the laser cavity using a fiber ferrule where light interacts with the material. Finally, the light was split into 90% and 10% using a 90:10 couplers; 90% was connected to the WDM to form the ring cavity, and the remaining 10 % was used for the analysis. The output laser was analyzed using optical

 doi:10.20944/preprints202603.1241.v1

spectrum analyzer (MS9710C, Anritsu and AQ6317B, Yokogawa, Tokyo, Japan), a digital oscilloscope (Wavesurfer 3054z, Teledyne LeCroy, New York, USA), an intensity autocorrelator (FR-103XL, Femtochrome, California, USA), an InGaAs photo-detector (PD-03, Taizhou Tonghe Laser technology co. LTD, Wenling, China), radio frequency (RF) spectrum analyzer (N9020A, Agilent, California, USA and R&S FPC1000, Jena, Germany) and a power meter (PM100D-S122C, Thorlabs, New Jersey, American).

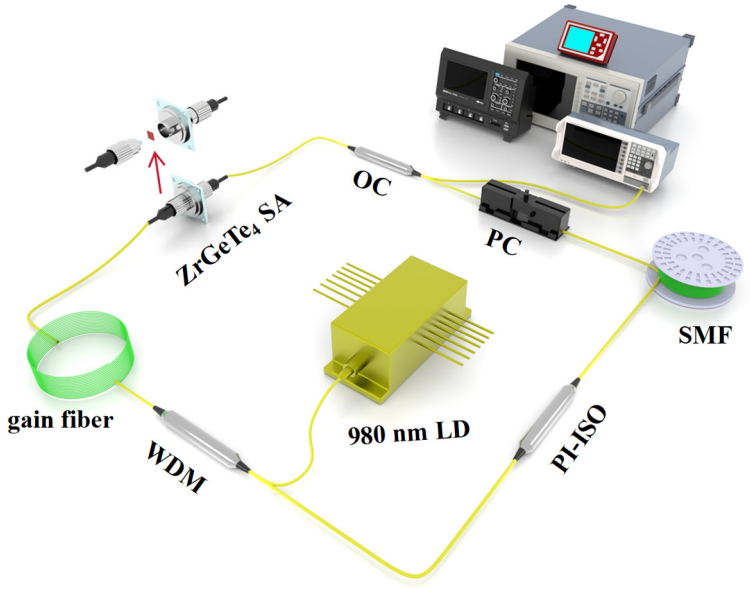

Figure 5. The experimental setup of the mode-locked laser.

4. Results and Discussion

At the beginning of the experiment, the Yb-doped fiber laser was operated without the integration of $ZrGeTe_4$-SA. In this configuration, mode-locked pulses were not detected, even when the pump power was gradually increased up to 800 mW and the PC was tuned. Then, $ZrGeTe_4$-SA was inserted into the fiber laser. By adjusting the PC and increasing the pump power, the stable mode-locked operation at a fundamental frequency of 24.85 MHz was achieved. Figure 6 shows the output characteristics of mode-locked operation.

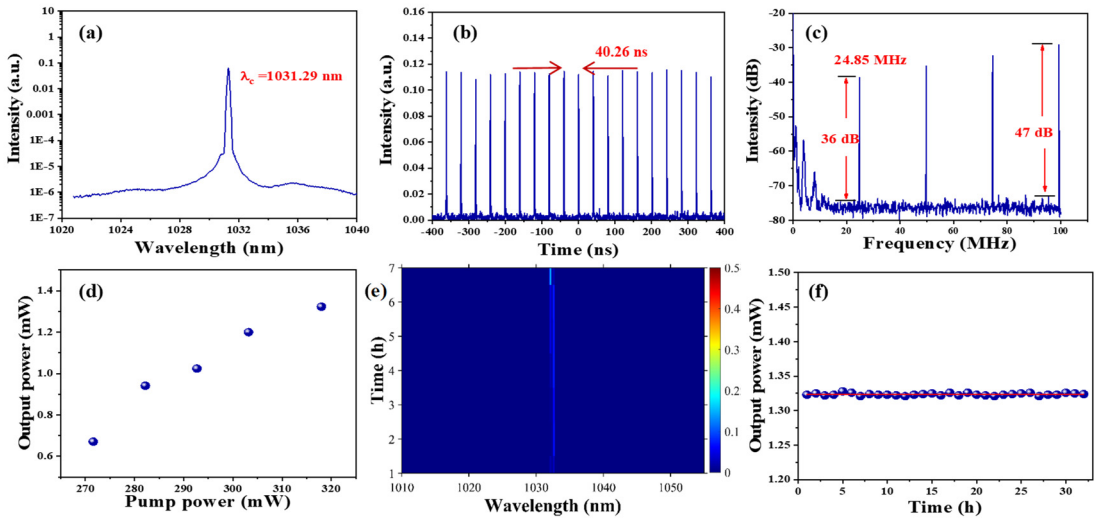

 doi:10.20944/preprints202603.1241.v1

Figure 6. The output characteristics of mode-locked operation at 1 μm. (a) Optical spectrum. (b) Pulse sequence. (c) RF spectrum. (d) Output power relative to pump power. (e) Optical spectrum in 6 h. (f) Output power variation during 32 h.

When the pump power is added to 272 mW, a mode-locked pulse of fundamental frequency at 24.85 MHz is detected. Figure 6a is its optical spectrum, and the central spectrum is located at 1031.29 nm. The pulse sequence diagram is shown in Figure 6b. The pulses are very stable, and the time interval between each pulse is 40.26 ns. The corresponding length of the laser cavity is approximately 8.27 m. The pulse width displayed by the oscilloscope is 786.3 ps. The radio frequency spectrum with a bandwidth of 100 MHz was tested, and the results are shown in Figure 6c. The signal-to-noise ratio (SNR) of the fundamental frequency mode-locked is 36 dB. The SNR of the fourth-order mode-locking is 47 dB. This indicates that the higher harmonics also exhibit good stability. As shown in Figure 6d, the mode-locking operation is achieved between 272 mW and 318 mW, with the output power linearly increasing from 0.67 mW to 1.32 mW. In addition, we also tested its long-term stability. Figure 6e and Figure 6f show the optical spectrum within 6 hours and the output power variation within 32 hours, respectively. All results indicate that the mode-locking operation is very stable.

In Er-doped fiber laser, when the pump power reaches the threshold of 52 mW, the traditional soliton mode-locking is achieved. As shown in Figure 7a, the central wavelength of the spectrum is 1561.10 nm, and it has a clearly symmetrical double Kelly sidebands, which is a typical feature of the normal formation of a traditional soliton in a laser cavity with anomalous dispersion. The full width at half maximum (FWHM) of the spectrum is 3.08 nm. The corresponding autocorrelation data at this point is Figure 7b, and after being fitted by sech² profile, the pulse width measured was 1.26 ps. Using the spectral pulse width, λ_c, and 3-dB bandwidth, the time-bandwidth product (TBP) was calculated to be 0.388, to some extent exceeding the transform-limited value of 0.315, indicating slight chirping. As shown in Figure 7c, the pulse train exhibits a stable pulse interval of 228.25 ns and a frequency of 4.38 MHz. This results correspond to a laser cavity length of 46.63 m. This result is also confirmed by the RF spectrum in Figure 7d. The SNR ratio of 59 dB indicates that the mode-locking operation of the laser is stable. In addition, the RF spectrum with a bandwidth of 2 GHz was also tested. The test results are shown in the inset of Figure 7d. This figure indicates that the higher harmonics exhibit good stability and long-term stability. These results confirm that the demonstration of achieving stable passive mode-locked pulses in Er-doped fiber laser by using $ZrGeTe_4$ SA is successful.

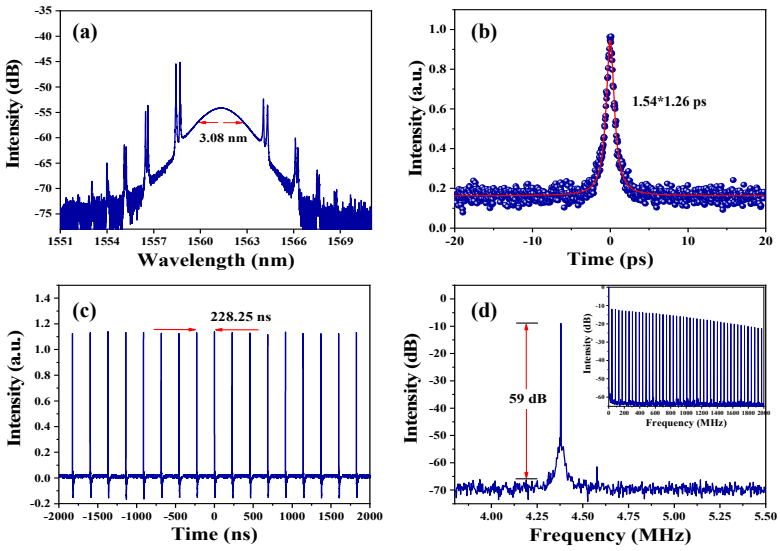

Figure 7. (a) Optical spectrum. (b) Autocorrelation trace by sech² fitting. (c) Pulse train. (d) RF spectrum.

 doi:10.20944/preprints202603.1241.v1

The stability of fiber lasers and ultrafast photonic devices is crucial in their applications. We monitored the long-term output power stability and output optical spectrum of mode-locked erbium-doped fiber laser under the pump power of 220 mW. As is shown in Figure 8a, at the threshold of 52 mW pump power, the output power in the mode-locked state is 0.35 mW. As the pump power increases to 220 mW, the laser output power also linearly increases to 0.45 mW. At the highest pump power of 220 mW, we tested the output power for 18 hours with minimal variation, as shown in Figure 8b. Figure 8c shows the variation of the output optics spectrum over a period of 15 hours, and the results indicate that the spectrum remains largely unchanged. Long term continuous testing has proven the stability and durability of $ZrGeTe_4$ photonic devices.

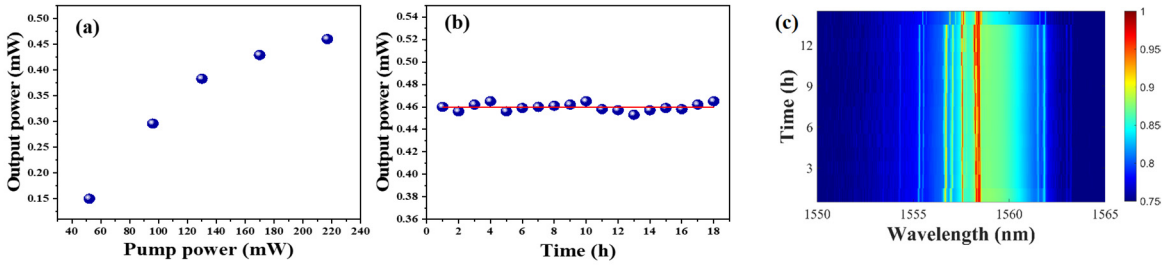

Figure 8. (a) Output power relative to pump power. (b) Output power variation during 18 h. (c) Optical spectrum in 15 h.

5. Conclusions

In conclusion, the nonlinear optical properties of $ZrGeTe_4$ at 1 μm were first detected, demonstrating its saturable absorption characteristics at 1 μm. We have demonstrated the fast response time of $ZrGeTe_4$-PVA thin film for the first time through pump-probe technology. The modulation depth of the $ZrGeTe_4$-PVA thin film SA in the 1 μm and 1.55 μm wavelength bands was 7.7% and 14.5%, respectively. By employing $ZrGeTe_4$ as a saturable absorber, a passive mode-locked fiber laser at the wavelength of 1031.29 nm was demonstrated for the first time. In the Yb-doped mode-locked fiber laser, stable pulses with a pulse repetition rate of 24.85 MHz under the excitation of 272 mW of pump power were achieved. In an erbium-doped fiber laser operating at a wavelength of 1561.10 nm, we measured a pulse width as short as 1.26 ps with a pulse repetition rate of 4.38 MHz. Expanding the application of $ZrGeTe_4$ saturable absorber to other wavelength regions such as 2 μm will also be considered to explore its broader photonic potential. It can be widely used in ultrafast photonics and optoelectronics in the future.

Author Contributions: Conceptualization, L.G.; methodology, N.X. and G.G.; software, Z.Z.; validation, H.Z.; formal analysis, W.Y.; investigation, L.S.; writing—original draft preparation, X.S. and W.Y.; visualization, M.Z.; writing—review and editing, X.S.; supervision, H.Z.; project administration, L.S.; funding acquisition, N.X. All authors have read and agreed to the published version of the manuscript.

Funding: This work was supported by the Shandong Province Natural Science Foundation (Grant nos. ZR2025QC23).

Data Availability Statement: Data underlying the results presented in this paper are not publicly available at this time but may be obtained from the authors upon reasonable request.

Conflicts of Interest: The authors declare no conflicts of interest.

References

1. Santos, H.D.A.; Gutiérrez, I.Z.; Shen, Y.-L.; Lifante, J.; Ximendes, E.; Laurenti, M.; Méndez-González, D.; Calderón, O.G.; Cabarcos, E.L.; Fernández, N.; Chaves-Coira, I.; Lucena-Agell, D.; Monge, L.; Mackenzie, M.D.; Marqués-Hueso, J.; Jones, C.M.S.; Jacinto, C.; del Rosal, B.; Kar, A.K.; Rubio-Retama, J.; Jaque, D.

 doi:10.20944/preprints202603.1241.v1

Ultrafast photochemistry produces superbright short-wave infrared dots for low-dose in vivo imaging. Nat. Commun. **2020**, 11, 2933.

2. Kerse, C.; Kalaycıoğluet, H.; Elahi, P.; Çetin, B. Kesim, D.K.; Akçaalan, Ö.; Yavas, S.; Aşık, M.D.; Öktem, B.; Hoogland, H.; Holzwarth, R.; Ilday, F. Ö. Ablation-cooled material removal with ultrafast bursts of pulses. Nature **2016**, 537, 84–88.
3. Liu, J.-T.; Yang, F.; Lu, J.-P.; Ye, S.; Guo, H.-W.; Nie, H.-K.; Zhang, J.-L.; He, J.-J.; Zhang, B.-T.; Ni, Z.-H. High output mode-locked laser empowered by defect regulation in 2D Bi_2O_2Se saturable absorber. Nat. Commun. **2022**, 13, 3855.
4. Zhang, L.; Tang, P.-H.; Zhu, J.-H.; Zhou, Z.-X.; Wu, H.-T.; Wang, Z.-H. Dynamic Behaviors of Pulsating Noise-like Pulses in an Ultrafast Fiber Laser. Photonics **2025**, 12, 937.
5. Boussafa, Y.; Sader, L.; Hoang, V.T.; Chaves, B.P.; Bougaud, A.; Fabert, M.; Tonello, A.; Dudley, J.M.; Kues, M.; Wetzel, B. Deep learning prediction of noise-driven nonlinear instabilities in fibre optics. Nat. Commun. **2025**, 16, 7800.
6. Zhang, X.-F.; Zhang, F.; Jia, K.-P.; Liu, Y.-F.; Shi, H.-S.; Jiang, Y.-Y.; Jiang, X.-H.; Ma, L.-S.; Liang, W.; Xie, Z.-D.; Zhu, S.-N. Miniature narrow-linewidth 1 μm laser. Appl. Phys. Lett. **2024,** 124, 1311901.
7. Wang, H.-J.; Zhu, X.-Y.; Weng, X.-B.; Deng, L.-X.; Zheng, Y.-T.; Shen, Z.-H.; You, H.-Y.; Tang, H.-J.; Dong, X.; Li, M.-Y.; Bai, S.-C.; Dong, J.; He, H.-S. Hand-held laser for miniature photoacoustic microscopy: triggerable, millimeter scale, cost-effective, and functional. Photon. Res. **2025**, 13, 1637-1646.
8. Subramaniam, T.K. Erbium doped fiber lasers for long distance communication using network of fiber optics. Am. J. Opt. Photonics **2015**, 3, 34.
9. Zhang, H.-Z.; Du, Y.-Q.; Zeng, C.; Sun, Z.-P.; Zhang, Y.; Zhao, J.-L.; Mao, D. The dissipative Talbot soliton fiber laser. Sci. Adv. **2024**, 10, eadl2125.
10. Zhang, Z.-X.; Luo, M.; Liu, J.-H.; Yang, Y.-T.; Li, T.-J.; Liu, M.; Luo, A.-P.; Xu, W.-C.; Luo, Z.-C. Coherence-controlled chaotic soliton bunch. Nat. Commun. **2024**, 15, 6148.
11. Wang, Z.-H.; Zhu, J.-H.; Ji, Y.-B.; Liu, J.; Song, Y.-F. Versatile pulses and dynamic evolution in a 1.7-μm ultrafast Tm-doped fiber laser. Opt. Commun. **2025**, 596, 132419.
12. Paradis, P.; Fortin, V.; Aydin, Y.O.; Vallée, R.; Bernier, M. 10 W-level gain-switched all-fiber laser at 2.8 μm. Opt. Lett. **2018**, 43, 3196-3199.
13. Lü, X.-Y.; Han, Q.; Liu, T.-G.; Chen, Y.-F.; Ren, K. Actively Q-switched erbium-doped fiber ring laser with a nanosecond ceramic optical switch. Laser Phys. **2014**, 24, 115102.
14. Cuadrado-Laborde, C.; Diez, A.; Delgado-Pinar, M.; Cruz, J.L.; Andrés, M.V. Mode locking of an all-fiber laser by acousto-optic superlattice modulation. Opt. Lett. **2009**, 34, 1111-1113.
15. El-Sherif, A.F.; King, T.A. High-energy, high-brightness Q-switched Tm^{3+}-doped fiber laser using an electro-optic modulator. Opt. Commun. **2003**, 218, 337-344.
16. 16.Zhang, H.-N.; Sun, S.; Shang, X.-X.; Guo, B.; Li, X.-H.; Chen, X.-H.; Jiang, S.-Z.;Zhang, H.; Agren, H.; Zhang, W.-F.; Wang, G.-M.; Lu, C.; Fu, S.-G. Ultrafast photonics applications of emerging 2D-Xenes beyond graphene. Nanophotonics **2022**, 11, 1261-1284.
17. Guo, B.; Xiao, Q.-L.; Wang, S.-H.; Zhang, H. 2D layered materials: synthesis, nonlinear optical properties, and device applications. Laser Photonics Rev. **2019**, 13, 1800327.
18. Shang, X.-X.; Xu, N.-N.; Zhang, H.-N.; Li, D.-W. Nonlinear photoresponse of high damage threshold titanium disulfide nanocrystals for Q-switched pulse generation. Opt. Laser Technol. **2022**, 151, 107988.
19. Xu, N.-N.; Sun, S.; Shang, X.-X.; Zhang, H.-N.; Li, D.-W. Harmonic and fundamental-frequency mode-locked operations in an Er-doped fiber laser using a $Cr_2Si_2Te_6$-based saturable absorber. Opt. Mater. Express **2022**, 12, 166-173.
20. Li, X.-H.; Huang, X.-Z.; Han, Y.-H.; Chen, E.-C.; Guo, P.-L.; Zhang, W.-N.; An, M.-Q.; Pan, Z.-W.; Xu, Q.; Guo, X.-X.; Huang, X.-W.; Wang, Y.-S.; Zhao, W. High-performance γ-MnO_2 Dual-Core, Pair-Hole Fiber for Ultrafast Photonic. Ultrafast Sci. **2023**, 3, 0006.
21. Li, L.; Cheng, J.-W.; Zhao, Q.-Y.; Zhang, J.-N.; Yang, H.-R.; Zhang, Y.-M.; Hui, Z.-Q.; Zhao, F.; Liu, W.-J. Chromium oxide film for Q-switched and mode-locked pulse generation. Opt. Express **2023**, 31, 16872-16881.

 doi:10.20944/preprints202603.1241.v1

22. Shang, X.-X.; Xu, N.-N.; Guo, J.; Sun, S.; Zhang, H.-N.; Wageh, S.; Al-Ghamdi, A.A.; Zhang, H.; Li, D.-W. Niobium telluride absorber for a mode-locked vector soliton fiber laser. Sci. China. Phys. Mech. **2023**, 66, 254211.
23. Cai, E.; Zhang, S.-Y.; Li, T.; Chen, M. Investigating high-energy Hermite–Gaussian and vortex laser generation in alexandrite. High Power Laser Sci. **2025,** 13, e43.
24. Pan, H.; Chu, H.-W.; Li, Y.; Pan, Z.-B.; Zhao, J.; Zhao, S.-Z.; Huang, W.-C.; Li, D. Bismuthene quantum dots integrated D-shaped fiber as saturable absorber for multi-type soliton fiber lasers. J. Materiomics **2023**, 9, 183-190.
25. Guo, P.-S.; Liang, J.; Zhou, B.-L.; Wang, W.-K.; Liu, Z.-R. Strong anisotropy and layer-dependent carrier mobility of two-dimensional semiconductor $ZrGeTe_4$. J. Phys-Condens Mat. **2020**, 32, 325502.
26. Adam, M.L.; Moses, O.A.; ur Rehman, Z.; Liu, Z.-F.; Song, L.; Wu, X.-J. Band gap engineering of monolayer $ZrGeTe_4$ via strain: A first-principles study. Mater. Chem. Phys. **2020**, 253, 123308.
27. Yan, W.; Johnson, B.C.; Balendhran, S.; Cadusch, J.; Yan, D.; Michel, J.I.; Wang, S.-F.; Zheng, T.; Crozier, K.; Bullock, J. Visible to Short-Wave Infrared Photodetectors Based on $ZrGeTe_4$ van der Waals Materials. ACS Appl. Mater. Interfaces **2021**, 13, 45881-45889.
28. Xu, B.-B.; Shi, L.; Ma, X.-G.; Zhang, H.-N.; Jiang, K.; Wang, J.; Chu, H.-W.; Tang, W.-J.; Xia, W. Investigations of the nonlinear optical properties of ZrGeTe4 nanosheets and their application in ultrafast photonics. J. Mater. Chem. C **2023**, 11, 13561-13569.
29. Gong, W.-T.; Li, L.; Gong, P.-L.; Zhou, Y.-L.; Zhang, Z.-T.; Zhou, W.-C.; Wang, W.-K.; Liu, Z.-R.; Tang, D.-S. Raman investigation of layered $ZrGeTe_4$ semiconductor. Appl. Phys. Lett. **2019**, 114, 172104.
30. Xue, Y.-J.; Li, H.-Q.; Wu, D.-H.; Yu, J.; Wang, J.; Jiang, K.; Zhang, H.-N.; Tang, W.-J.; Xia, W. Large-energy operation of an Er-doped fiber laser with $ZrGeTe_4$ saturable absorber. Opt. Fiber Technol. **2024**, 88, 103976.
31. Fan, W.-Y.; Han, Y.-N.; He, Y.-T.; Wang, L.-Z.; Wang, G.-M.; Bai, C.-X.; Zhang, W.-F.; Lu, C.; Qu, W.; Fu, S.-G.; Zhang, H.-N. Controllable and abundant soliton states from an all-fiber laser based on a $ZrGeTe_4$ saturable absorber. Opt. Mater. Express **2023**, 13, 3252-3265.